H. Ozoe

A. Mouri

M. Hiramitsu

Department of Industrial and Mechanical
Engineering,
School of Engineering,
Okayama University,
Okayama 700 Japan

S. W. Churchill

Department of Chemical Engineering,
University of Pennsylvania,
Philadelphia, PA 19104 U.S.A.

N. Lior

Department of Mechanical Engineering and
Applied Mechanics,
University of Pennsylvania,
Philadelphia, PA 19104 U.S.A.

Numerical Calculation of Three-Dimensional Turbulent Natural Convection in a Cubical Enclosure Using a Two-Equation Model for Turbulence

This paper presents a model and numerical results for turbulent natural convection in a cubical enclosure heated from below, cooled on a portion of one vertical side wall and insulated on all other surfaces. Three-dimensional balances were derived for material, energy, and the three components of momentum, as well as for the turbulent kinetic energy k and the rate of dissipation of turbulent kinetic energy ϵ. The constants used in the model were the same as those used by Fraikin et al. for two-dimensional convection in a channel. Illustrative transient calculations were carried out for $Ra = 10^6$ and 10^7 and $Pr = 0.7$. Both the dominant component of the vector potential and the Nusselt number were found to converge to a steady state. Isothermal lines and velocity vectors for vertical cross sections normal to the cooled wall indicated three-dimensional effects near the side walls. A top view of the velocity vectors revealed a downward spiral flow near the side walls along the cooled vertical wall. A weak spiral flow was also found along the side walls near the wall opposing the partially cooled one. The highest values of the eddy diffusivity were 2.6 and 5.8 times the molecular kinematic viscosity for $Ra = 10^6$ and 10^7, respectively. A coaxial double spiral movement, similar to that previously reported for laminar natural convection, was found for the time-averaged flow field. This computing scheme is expected to be applicable to other thermal boundary conditions.

1 Introduction

Turbulent natural convection is observed in many circumstances. The primary aim of this work was to study natural convection in large enclosures such as passive solar rooms with a heated floor and a cooled window. The method is also expected to be useful for turbulent natural convection in other applications such as for the equalization of temperature in a large nuclear reactor containment filled with fluid, and for removal of the heat generated within the casing of electronic equipment by integrated circuits. Natural convection in such applications necessarily becomes turbulent and three-dimensional due to the large scale of a solar room and/or the large temperature difference. Prior numerical calculations of turbulent natural convection have been limited primarily to boundary-layer flow and to two-dimensional flows in enclosures.

Turbulent free convection in the boundary layer along a vertical heated plate in an unconfined fluid has been computed by Plumb and Kennedy [1] and Lin and Churchill [2] using a two-equation model, and by Fujii and Fujii [3] using a Glushko model. Farouk and Güceri [4] computed turbulent free convection about a horizontal cylinder in an unconfined fluid using a $k-\epsilon$ model developed for forced convection.

Turbulent natural convection in a square channel with isothermally heated and cooled vertical walls and linear temperature profiles along the lower and upper horizontal boundaries was computed by Fraikin et al. [5], also using a two-equation model. Their calculations were for air at Grashof numbers of 10^7, 5×10^7, and 10^8, which they postulated to be in the turbulent regime. Their maximum computed turbulent viscosity ranged from 4 times the molecular

viscosity at Gr $= 10^7$ to 9.6 times at 10^8. They carried out a sensitivity analysis of several of the constants in the $k-\epsilon$ model. Perturbation of $\pm 10-20$ percent for the constants in the model caused $\pm 40-50$ percent changes in the turbulent properties but only 10 percent or less in the Nusselt number. However, this result may be limited to their specific boundary conditions.

Farouk and Güceri [6] calculated turbulent natural convection for Ra up to 10^7 using a $k-\epsilon$ model in cylindrical coordinates for a horizontal concentric annulus whose inner cylinder was heated and outer cylinder cooled. They pointed out that at higher Rayleigh numbers a finer grid size would be necessary to compute the thin boundary layer next to the walls.

Ozoe et al. [7] developed a computing scheme using a $k-\epsilon$ model for two-dimensional turbulent natural convection in a long square channel heated on one vertical wall, cooled on the opposite one, and thermally insulated along the upper and lower horizontal walls. They carried out computations for water for Rayleigh numbers up to 10^{11} and obtained good agreement with experimental values for the overall Nusselt number and fair agreement for the time-averaged vertical velocity. The latter agreement was improved by using modified values for the empirical constants in the $k-\epsilon$ model as identified through a sensitivity analysis.

A primary objective of the present study was to develop a program for characterizing the heat transfer in a passive solar room which invokes three-dimensional turbulent natural convection. A cubical enclosure was chosen for modeling with the floor heated and part of one of the vertical walls cooled to simulate a window. This model also simulates natural convective cooling of the casing of electronic equipment. The two-dimensional computing scheme developed and verified experimentally by Ozoe et al. [7] was utilized for this three-dimensional problem.

2 Turbulent Mathematical Model

A direct extension of the two-dimensional mathematical model for turbulent natural convection used by Fraiklin et al. [5], Farouk and Güceri [6], and Ozoe et al. [7] was used in this three-dimensional investigation. As reported by Ozoe et al. [7], the k–ϵ model proposed for low-Reynolds-number flow by Jones and Launder [8] was found to produce a numerically unstable solution for natural convection in a two-dimensional channel and was therefore not employed herein.

The following seven equations represent in order and in dimensionless form the conservation of time-averaged momentum in the X, Y, and Z directions, of material, of energy, of turbulent kinetic energy, and of the rate of dissipation of turbulent kinetic energy.

The angle of inclination ϕ of the X axis from a horizontal plane about the horizontal Y axis was included in the equations. However, this angle of inclination was set to zero in the sample calculations in this work.

$$\frac{\partial U}{\partial \tau} + U \frac{\partial U}{\partial X} + V \frac{\partial U}{\partial Y} + W \frac{\partial U}{\partial Z}$$

$$= \frac{\partial}{\partial X}\left[(\sigma + \nu_t^*)\left(\frac{\partial U}{\partial X} + \frac{\partial U}{\partial X}\right)\right] + \frac{\partial}{\partial Y}\left[(\sigma + \nu_t^*)\left(\frac{\partial U}{\partial Y}\right.\right. \quad (1)$$

$$\left.\left. + \frac{\partial V}{\partial X}\right)\right] + \frac{\partial}{\partial Z}\left[(\sigma + \nu_t^*)\left(\frac{\partial U}{\partial Z} + \frac{\partial W}{\partial X}\right)\right] + \sigma\, T \sin \phi$$

$$- \frac{\partial}{\partial X}\left(P + \frac{2}{3} K\right)$$

$$\frac{\partial V}{\partial \tau} + U \frac{\partial V}{\partial X} + V \frac{\partial V}{\partial Y} + W \frac{\partial V}{\partial Z} = \frac{\partial}{\partial X}\left[(\sigma + \nu_t^*)\left(\frac{\partial V}{\partial X}\right.\right.$$

$$\left.\left. + \frac{\partial U}{\partial Y}\right)\right] + \frac{\partial}{\partial Y}\left[(\sigma + \nu_t^*)\left(\frac{\partial V}{\partial Y} + \frac{\partial V}{\partial Y}\right)\right] + \frac{\partial}{\partial Z}\left[(\sigma\right.$$

$$\left. + \nu_t^*)\left(\frac{\partial V}{\partial Z} + \frac{\partial W}{\partial Y}\right)\right] - \frac{\partial}{\partial Y}\left(P + \frac{2}{3} K\right) \quad (2)$$

$$\frac{\partial W}{\partial \tau} + U \frac{\partial W}{\partial X} + V \frac{\partial W}{\partial Y} + W \frac{\partial W}{\partial Z} = \frac{\partial}{\partial X}\left[(\sigma + \nu_t^*)\left(\frac{\partial W}{\partial X}\right.\right.$$

$$\left.\left. + \frac{\partial U}{\partial Z}\right)\right] + \frac{\partial}{\partial Y}\left[(\sigma + \nu_t^*)\left(\frac{\partial W}{\partial Y} + \frac{\partial V}{\partial Z}\right)\right] + \frac{\partial}{\partial Z}\left[(\sigma\right.$$

$$\left. + \nu_t^*)\left(\frac{\partial W}{\partial Z} + \frac{\partial W}{\partial Z}\right)\right] - \sigma\, T \cos \phi - \frac{\partial}{\partial Z}\left(P + \frac{2}{3} K\right) \quad (3)$$

$$\frac{\partial U}{\partial X} + \frac{\partial V}{\partial Y} + \frac{\partial W}{\partial Z} = 0 \quad (4)$$

$$\frac{\partial T}{\partial \tau} + U \frac{\partial T}{\partial X} + V \frac{\partial T}{\partial Y} + W \frac{\partial T}{\partial Z} = \frac{\partial}{\partial X}\left[\left(1 + \frac{\nu_t^*}{\sigma_t}\right)\frac{\partial T}{\partial X}\right]$$

$$+ \frac{\partial}{\partial Y}\left[\left(1 + \frac{\nu_t^*}{\sigma_t}\right)\frac{\partial T}{\partial Y}\right] + \frac{\partial}{\partial Z}\left[\left(1 + \frac{\nu_t^*}{\sigma_t}\right)\frac{\partial T}{\partial Z}\right] \quad (5)$$

$$\frac{\partial K}{\partial \tau} + U \frac{\partial K}{\partial X} + V \frac{\partial K}{\partial Y} + W \frac{\partial K}{\partial Z} = \left(\sigma + \frac{\nu_t^*}{\sigma_k}\right)\left(\frac{\partial^2 K}{\partial X^2}\right.$$

$$\left. + \frac{\partial^2 K}{\partial Y^2} + \frac{\partial^2 K}{\partial Z^2}\right) + \frac{1}{\sigma_k}\left(\frac{\partial \nu_t^*}{\partial X} \frac{\partial K}{\partial X} + \frac{\partial \nu_t^*}{\partial Y} \frac{\partial K}{\partial Y}\right.$$

$$\left. + \frac{\partial \nu_t^*}{\partial Z} \frac{\partial K}{\partial Z}\right) + \nu_t\left[\left(\frac{\partial U}{\partial Y} + \frac{\partial V}{\partial X}\right)^2 + \left(\frac{\partial V}{\partial Z} + \frac{\partial W}{\partial Y}\right)^2\right.$$

$$\left. + \left(\frac{\partial W}{\partial X} + \frac{\partial U}{\partial Z}\right)^2 + 2\left(\frac{\partial U}{\partial X}\right)^2 + 2\left(\frac{\partial V}{\partial Y}\right)^2 + 2\left(\frac{\partial W}{\partial Z}\right)^2\right]$$

$$- E - \sigma \frac{\nu_t^*}{\sigma_t}\left(\frac{\partial T}{\partial X} \sin \phi - \frac{\partial T}{\partial Z} \cos \phi\right) \quad (6)$$

$$\frac{\partial E}{\partial \tau} + U \frac{\partial E}{\partial X} + V \frac{\partial E}{\partial Y} + W \frac{\partial E}{\partial Z} = \left(\sigma + \frac{\nu_t^*}{\sigma_\epsilon}\right)\left(\frac{\partial^2 E}{\partial X^2} + \frac{\partial^2 E}{\partial Y^2}\right.$$

$$\left. + \frac{\partial^2 E}{\partial Z^2}\right) + \frac{1}{\sigma_\epsilon}\left(\frac{\partial \nu_t^*}{\partial X} \frac{\partial E}{\partial X} + \frac{\partial \nu_t^*}{\partial Y} \frac{\partial E}{\partial Y} + \frac{\partial \nu_t^*}{\partial Z} \frac{\partial E}{\partial Z}\right)$$

$$+ C_1 \frac{E}{K} \nu_t^*\left[\left(\frac{\partial U}{\partial Y} + \frac{\partial V}{\partial X}\right)^2 + \left(\frac{\partial V}{\partial Z} + \frac{\partial W}{\partial Y}\right)^2\right.$$

$$\left. + \left(\frac{\partial W}{\partial X} + \frac{\partial U}{\partial Z}\right)^2 + 2\left(\frac{\partial U}{\partial X}\right)^2 + 2\left(\frac{\partial V}{\partial Y}\right)^2 + 2\left(\frac{\partial W}{\partial Z}\right)^2\right]$$

$$- C_2 \frac{E^2}{K} - C_\epsilon \sigma \frac{E}{K}\left(\frac{\partial T}{\partial X} \sin \phi - \frac{\partial T}{\partial Z} \cos \phi\right)\frac{\nu_t^*}{\sigma_t} \quad (7)$$

The dimensionless eddy diffusivity is related as follows, per Jones and Launder [8], to the dimensionless time-averaged turbulent kinetic energy and the dimensionless time-averaged rate of dissipation of turbulent kinetic energy

Nomenclature

c_1 = parameter in k–ϵ model
c_2 = parameter in k–ϵ model
c_D = constant = $C_\mu^{3/4}$
c_μ = parameter in k–ϵ model
c_ϵ = parameter in k–ϵ model
D = y length of the enclosure, m
E = dimensionless time-averaged rate of dissipation of turbulent kinetic energy = $\epsilon/(\alpha^3 \mathrm{Ra}_L^{4/3}/L^4)$
g = acceleration due to gravity, m/s^2
H = height of the enclosure, m
$\bar{H}$ = dimensionless height of the enclosure = $\mathrm{Ra}_H^{1/3}$
K = dimensionless time-averaged turbulent kinetic energy = $k/[(\alpha/L)\mathrm{Ra}_L^{1/3}]^2$
k = turbulent kinetic energy = $(\overline{u'^2} + \overline{v'^2} + \overline{w'^2})/2$, m^2/s^2
L = x length of the enclosure, m
l = length scale, m
l_m = Prandtl mixing length, m
n = normal direction, m
Nu = overall Nusselt number

p = time-averaged pressure, Pa
Pr = Prandtl number = ν/α
Ra_L = Rayleigh number = $g\beta(\theta_h - \theta_l)L^3/(\alpha\nu)$
T = dimensionless time-averaged temperature
t = time, s
U = dimensionless time-averaged velocity in x direction = $u/[(\alpha/L)\mathrm{Ra}_L^{1/3}]$
u = component of time-averaged velocity in x direction, m/s
V = dimensionless time-averaged velocity in y direction = $v/[(\alpha/L)\mathrm{Ra}_L^{1/3}]$
v = component of time-averaged velocity in y direction, m/s
W = dimensionless time-averaged velocity in z direction = $w/[(\alpha/L)\mathrm{Ra}_L^{1/3}]$
w = component of time-averaged velocity in z direction, m/s
X = dimensionless x coordinate = $x/(L/\mathrm{Ra}_L^{1/3})$
x = horizontal coordinate, m

$$v_t^* = C_\mu \frac{K^2}{E} \qquad (8)$$

The dimensionless time-averaged variables in the above equations are defined as

$$X = \frac{x}{x_0}, \quad Y = \frac{y}{y_0}, \quad Z = \frac{z}{z_0}, \quad U = \frac{u}{u_0}, \quad V = \frac{v}{v_0}, \quad W = \frac{w}{w_0},$$

$$\tau = \frac{t}{t_0}, \quad P = \frac{p}{p_0}, \quad K = \frac{k}{k_0}, \quad E = \frac{\epsilon}{\epsilon_0}, \quad T = \frac{\theta - \theta_0}{\theta_h - \theta_l},$$

$$v_t^* = \frac{v_t}{v_{t_0}}, \quad x_0 = y_0 = z_0 = \left[\frac{g\beta(\theta_h - \theta_l)}{\alpha\nu}\right]^{-\frac{1}{3}} = \frac{L}{\mathrm{Ra}_L^{1/3}},$$

$$u_0 = v_0 = w_0 = \frac{\alpha}{x_0} = \frac{\alpha}{L} \mathrm{Ra}_L^{1/3}, \quad p_0 = \rho\alpha^2/x_0^2$$

$$= (\rho\alpha^2/L^2)\mathrm{Ra}_L^{2/3},$$

$$k_0 = \left(\frac{\alpha}{x_0}\right)^2 = \left(\frac{\alpha}{L}\mathrm{Ra}_L^{1/3}\right)^2,$$

$$\epsilon_0 = \alpha^3/x_0^4 = \alpha^3\mathrm{Ra}_L^{4/3}/L^4, \quad v_{t_0} = \alpha,$$

and

$$t_0 = \frac{x_0}{u_0} = L^2/(\mathrm{Ra}_L^{2/3}\alpha).$$

The equations for the conservation of momentum were cross-differentiated and subtracted to eliminate the pressure terms, resulting in the following three equations for the components of the vorticity

$$\frac{\partial\Omega_1}{\partial\tau} + U\frac{\partial\Omega_1}{\partial X} + V\frac{\partial\Omega_1}{\partial Y} + W\frac{\partial\Omega_1}{\partial Z} - \Omega_1\frac{\partial U}{\partial X} - \Omega_2\frac{\partial U}{\partial Y}$$

$$- \Omega_3\frac{\partial U}{\partial Z} = (\sigma + v_t^*)\left(\frac{\partial^2\Omega_1}{\partial X^2} + \frac{\partial^2\Omega_1}{\partial Y^2} + \frac{\partial^2\Omega_1}{\partial Z^2}\right) + \frac{\partial v_t^*}{\partial X}\frac{\partial\Omega_1}{\partial X}$$

$$+ 2\frac{\partial v_t^*}{\partial Y}\frac{\partial\Omega_1}{\partial Y} + 2\frac{\partial v_t^*}{\partial Z}\frac{\partial\Omega_1}{\partial Z} - \frac{\partial v_t^*}{\partial Y}\frac{\partial\Omega_2}{\partial X} - \frac{\partial v_t^*}{\partial Z}\frac{\partial\Omega_3}{\partial X}$$

$$- \left(\frac{\partial^2 v_t^*}{\partial Y^2} + \frac{\partial^2 v_t^*}{\partial Z^2}\right)\Omega_1 + \frac{\partial^2 v_t^*}{\partial X\partial Y}\Omega_2 + \frac{\partial^2 v_t^*}{\partial X\partial Z}\Omega_3$$

$$+ 2\left[\frac{\partial^2 v_t^*}{\partial X\partial Y}\frac{\partial W}{\partial X} + \frac{\partial^2 v_t^*}{\partial Y^2}\frac{\partial W}{\partial Y} + \frac{\partial^2 v_t^*}{\partial Y\partial Z}\frac{\partial W}{\partial Z}\right.$$

$$\left. - \left(\frac{\partial^2 v_t^*}{\partial X\partial Z}\frac{\partial V}{\partial X} + \frac{\partial^2 v_t^*}{\partial Y\partial Z}\frac{\partial V}{\partial Y} + \frac{\partial^2 v_t^*}{\partial Z^2}\frac{\partial V}{\partial Z}\right)\right]$$

$$- \sigma\frac{\partial T}{\partial Y}\cos\phi \qquad (9)$$

$$\frac{\partial\Omega_2}{\partial\tau} + U\frac{\partial\Omega_2}{\partial X} + V\frac{\partial\Omega_2}{\partial Y} + W\frac{\partial\Omega_2}{\partial Z} - \Omega_1\frac{\partial V}{\partial X} - \Omega_2\frac{\partial V}{\partial Y}$$

$$- \Omega_3\frac{\partial V}{\partial Z} = (\sigma + v_t^*)\left(\frac{\partial^2\Omega_2}{\partial X^2} + \frac{\partial^2\Omega_2}{\partial Y^2} + \frac{\partial^2\Omega_2}{\partial Z^2}\right) + 2\frac{\partial v_t^*}{\partial X}\frac{\partial\Omega_2}{\partial X}$$

$$+ \frac{\partial v_t^*}{\partial Y}\frac{\partial\Omega_2}{\partial Y} + 2\frac{\partial v_t^*}{\partial Z}\frac{\partial\Omega_2}{\partial Z} - \frac{\partial v_t^*}{\partial X}\frac{\partial\Omega_1}{\partial Y} - \frac{\partial v_t^*}{\partial Z}\frac{\partial\Omega_3}{\partial Y}$$

$$+ \frac{\partial^2 v_t^*}{\partial X\partial Y}\Omega_1 - \left(\frac{\partial^2 v_t^*}{\partial X^2} + \frac{\partial^2 v_t^*}{\partial Z^2}\right)\Omega_2 + \frac{\partial^2 v_t^*}{\partial Y\partial Z}\Omega_3$$

$$+ 2\left[\frac{\partial^2 v_t^*}{\partial X\partial Z}\frac{\partial U}{\partial X} + \frac{\partial^2 v_t^*}{\partial Y\partial Z}\frac{\partial U}{\partial Y} + \frac{\partial^2 v_t^*}{\partial Z^2}\frac{\partial U}{\partial Z}\right.$$

$$\left. - \left(\frac{\partial^2 v_t^*}{\partial X^2}\frac{\partial W}{\partial X} + \frac{\partial^2 v_t^*}{\partial X\partial Y}\frac{\partial W}{\partial Y} + \frac{\partial^2 v_t^*}{\partial X\partial Z}\frac{\partial W}{\partial Z}\right)\right]$$

$$+ \sigma\left(\frac{\partial T}{\partial Z}\sin\phi + \frac{\partial T}{\partial X}\cos\phi\right) \qquad (10)$$

$$\frac{\partial\Omega_3}{\partial\tau} + U\frac{\partial\Omega_3}{\partial X} + V\frac{\partial\Omega_3}{\partial Y} + W\frac{\partial\Omega_3}{\partial Z} - \Omega_1\frac{\partial W}{\partial X} - \Omega_2\frac{\partial W}{\partial Y}$$

$$- \Omega_3\frac{\partial W}{\partial Z} = (\sigma + v_t^*)\left(\frac{\partial^2\Omega_3}{\partial X^2} + \frac{\partial^2\Omega_3}{\partial Y^2} + \frac{\partial^2\Omega_3}{\partial Z^2}\right) + 2\frac{\partial v_t^*}{\partial X}\frac{\partial\Omega_3}{\partial X}$$

$$+ 2\frac{\partial v_t^*}{\partial Y}\frac{\partial\Omega_3}{\partial Y} + \frac{\partial v_t^*}{\partial Z}\frac{\partial\Omega_3}{\partial Z} - \frac{\partial v_t^*}{\partial X}\frac{\partial\Omega_1}{\partial Z} - \frac{\partial v_t^*}{\partial Y}\frac{\partial\Omega_2}{\partial Z}$$

$$+ \frac{\partial^2 v_t^*}{\partial X\partial Z}\Omega_1 + \frac{\partial^2 v_t^*}{\partial Y\partial Z}\Omega_2 - \left(\frac{\partial^2 v_t^*}{\partial X^2} + \frac{\partial^2 v_t^*}{\partial Y^2}\right)\Omega_3$$

$$+ 2\left[\frac{\partial^2 v_t^*}{\partial X^2}\frac{\partial V}{\partial X} + \frac{\partial^2 v_t^*}{\partial X\partial Y}\frac{\partial V}{\partial Y} + \frac{\partial^2 v_t^*}{\partial X\partial Z}\frac{\partial V}{\partial Z}\right.$$

Nomenclature (cont.)

Y = dimensionless y coordinate = $y/(L/\mathrm{Ra}_L^{1/3})$

y = horizontal coordinate, m

Z = dimensionless vertical coordinate = $z/(L/\mathrm{Ra}_L^{1/3})$

z = vertical coordinate, m

α = thermal diffusivity, m²/s

α_t = eddy diffusivity for heat transfer, m²/s

β = volumetric coefficient of expansion with temperature, K⁻¹

ϵ = time-averaged rate of dissipation of turbulent kinetic energy, m²/s³

θ = temperature, K

θ_0 = = $(\theta_h + \theta_l)/2$, K

κ = von Karman's constant = 0.42

μ = viscosity, Pa•s

ν = kinematic viscosity = μ/ρ, m²/s

ν_t = eddy diffusivity, m²/s

ν_t^* = dimensionless eddy diffusivity = $\nu_t/\alpha = c_\mu K^2/E$

ρ = density, kg/m³

σ = Prandtl number = ν/α

σ_K = Prandtl number for the turbulent kinetic energy

σ_t = turbulent Prandtl number = ν_t/α_t

σ_ϵ = Prandtl number for the rate of dissipation of turbulent kinetic energy

τ = dimensionless time = $t/[L^2/(\mathrm{Ra}_L^{2/3}\alpha)]$

τ_w = wall shear stress, N/m²

ϕ = angle of inclination of the X axis of the cube from a horizontal plane about the horizontal Y axis

ψ_i = dimensionless time-averaged vector potential

Ω_i = dimensionless time-averaged vorticity

Subscripts

0 = dimensional reference value

$1, 2, 3$ = empirical constants of turbulent model, or x, y, and z directions

c = center or central-plane value

H = height as a reference value

h = heated wall

L = width as a reference value

l = cooled wall

$$-\left(\frac{\partial^2 \nu_t^*}{\partial X \partial Y}\frac{\partial U}{\partial X}+\frac{\partial^2 \nu_t^*}{\partial Y^2}\frac{\partial U}{\partial Y}+\frac{\partial^2 \nu_t^*}{\partial Y \partial Z}\frac{\partial U}{\partial Z}\right)\Big]$$

$$-\sigma\frac{\partial T}{\partial Y}\sin\phi \qquad (11)$$

The dimensionless vorticity is here defined as follows:

$$\Omega=\begin{bmatrix}\Omega_1\\[4pt]\Omega_2\\[4pt]\Omega_3\end{bmatrix}=\begin{bmatrix}\dfrac{\partial W}{\partial Y}-\dfrac{\partial V}{\partial Z}\\[8pt]\dfrac{\partial U}{\partial Z}-\dfrac{\partial W}{\partial X}\\[8pt]\dfrac{\partial V}{\partial X}-\dfrac{\partial U}{\partial Y}\end{bmatrix} \qquad (12)$$

The three-dimensional vector potential is related to the velocity vector as follows, thereby automatically satisfying the continuity equation:

$$\mathbf{V}=\begin{bmatrix}U\\[4pt]V\\[4pt]W\end{bmatrix}=\begin{bmatrix}\dfrac{\partial\psi_3}{\partial Y}-\dfrac{\partial\psi_2}{\partial Z}\\[8pt]\dfrac{\partial\psi_1}{\partial Z}-\dfrac{\partial\psi_3}{\partial X}\\[8pt]\dfrac{\partial\psi_2}{\partial X}-\dfrac{\partial\psi_1}{\partial Y}\end{bmatrix} \qquad (13)$$

The vector potential is presumed to be solenoidal ($\nabla\cdot\psi = 0$), and the vector potential is therefore related to vorticity as follows:

$$\Omega=\nabla\times\mathbf{V}=-\nabla^2\psi \qquad (14)$$

Ozoe et al. [7] performed a sensitivity analysis for the constants of k–ϵ turbulent model and determined different values for C_1 and σ_t rather than those listed below. However, since the applicability of these values for different geometric and thermal boundary conditions is not known, they were not employed herein. The following empirical constants recommended by Launder and Spalding [9] were used, except for C_ϵ in the buoyant term of the E equation, which was adopted from Fraikin et al. [5]: $C_\mu = 0.09$, $C_1 = 1.44$, $C_2 = 1.92$, $C_\epsilon = 0.7$, $\sigma_K = 1$, $\sigma_\epsilon = 1.3$, and $\sigma_t = 1$.

The boundary conditions for the cubic room shown in Fig. 1 are summarized as follows:

1 Temperature

$T=0.5$ at $Z = \mathrm{Ra}_H^{1/3} = \overline{H}$

$T=-0.5$ for $Z = 0.106\overline{H}$ to $0.679\overline{H}$ at $X = 0$.

$\partial T/\partial n = 0$ on all other walls.

2 Velocity

All components of the velocity are zero on the wall, i.e.,

$U=V=W=0$ at $X=0$ and $\mathrm{Ra}_H^{1/3}(L/H)$

$\qquad\qquad\quad Y=0$ and $\mathrm{Ra}_H^{1/3}(D/H)$ (15)

$\qquad\qquad\quad Z=0$ and $\mathrm{Ra}_H^{1/3}$

3 Vorticity

The components of vorticity are extrapolated from the fluid velocity at one time step earlier. (This approximation holds rigorously at the final steady state.) Thus

$$\Omega_1=0,\ \Omega_2=-\frac{\partial W}{\partial X},\ \Omega_3=\frac{\partial V}{\partial X}\ \text{at}\ X=0\ \text{and}\ \mathrm{Ra}_H^{1/3}\,(L/H)$$

$$\Omega_1=\frac{\partial W}{\partial Y},\ \Omega_2=0,\ \Omega_3=-\frac{\partial U}{\partial Y}\ \text{at}\ Y=0\ \text{and}\ \mathrm{Ra}_H^{1/3}\,(D/H)$$

$\qquad\qquad\qquad\qquad\qquad\qquad\qquad\qquad\qquad (16)$

$$\Omega_1=-\frac{\partial V}{\partial Z},\ \Omega_2=\frac{\partial U}{\partial Z},\ \Omega_3=0\ \text{at}\ Z=0\ \text{and}\ \mathrm{Ra}_H^{1/3}$$
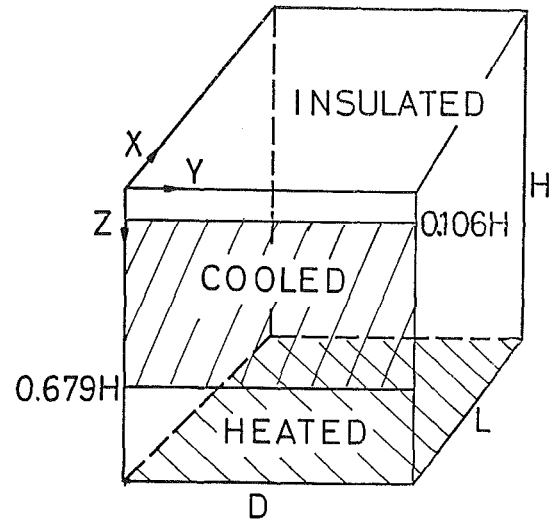

Fig. 1 Thermal boundary conditions for illustrative calculations for a cubical box

4 Vector potential

The following boundary conditions by Hirasaki and Hellums [10] for a rigid wall were adopted

$$\frac{\partial\psi_1}{\partial X}=\psi_2=\psi_3=0\ \text{at}\ X=0\ \text{and}\ \mathrm{Ra}_H^{1/3}\,(L/H)$$

$$\psi_1=\frac{\partial\psi_2}{\partial Y}=\psi_3=0\ \text{at}\ Y=0\ \text{and}\ \mathrm{Ra}_H^{1/3}\,(D/H) \qquad (17)$$

$$\psi_1=\psi_2=\frac{\partial\psi_3}{\partial Z}=0\ \text{at}\ Z=0\ \text{and}\ \mathrm{Ra}_H^{1/3}$$

5 Dimensionless turbulent kinetic energy K

The turbulent kinetic energy K was set to zero on all of the walls.

6 Rate of dissipation of dimensionless turbulent kinetic energy E

The rate of dissipation of turbulent kinetic energy is proportional to $k^{3/2}/l$, where l is a characteristic length expressing the scale of the turbulence. Since both k and l are zero on the wall, the value of ϵ is indeterminant. However, the rate of dissipation ϵ at a short distance from the wall can be derived as follows according to Kawamura [11]. First, let

$$\epsilon=C_D\,\frac{k^{3/2}}{l} \qquad (18)$$

where C_D is an unknown constant to be decided. Near the wall the characteristic length can be taken as equal to the Prandtl mixing length $l_m = l = \kappa y$ where y is the distance from the wall. Since $\tau_w = \rho\nu_t\,du/dy$ and $\nu_t = l_m^2\,du/dy$, $du/dy = u^*/l_m$ where u^* is the friction velocity $\sqrt{\tau_w/\rho}$. Then $\nu_t = l_m u^*$ and $\nu_t = C_\mu k^2/\epsilon = C_\mu k^{1/2}l_m/C_D$. Hence $k = (C_D u^*/C_\mu)^2$. Presuming local equilibrium, i.e., a rate of production equal to the rate of dissipation, then gives $|u'v'|\,du/dy = \nu_t\,(du/dy)^2 = \epsilon$. Finally considering $\nu_t = C_\mu k^2/\epsilon$ and $du/dy = u^*/l$, we get $k = C_\mu\,(u^*)^2/C_D^2$. Hence $C_D = C_\mu^{3/4}$ and $\epsilon_{\Delta y} = C_\mu^{3/4}k^{3/2}/(\kappa\,\Delta y)$ at $y = \Delta y$. Fraikin et al. [5] used this approximation, although they did not describe the derivation in detail.

The E equation was solved only in a reduced region excluding the walls. A finite-difference approximation was developed for equations (5) to (7) and (9) to (12), using a first-order forward approximation for the time step and a second-order central difference for the length derivatives.

According to Ozoe et al. [7] too coarse a grid size in comparison to the velocity resulted in too large a cell Reynolds
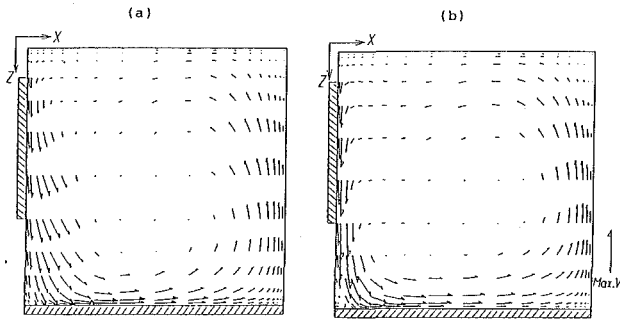
Fig. 2 Computed velocity vectors in vertical planes normal to the heated and cooled walls at Ra = 10^7 and Pr = 0.7: (a) Y = 0.05$\bar{H}$; (b) Y = 0.5$\bar{H}$
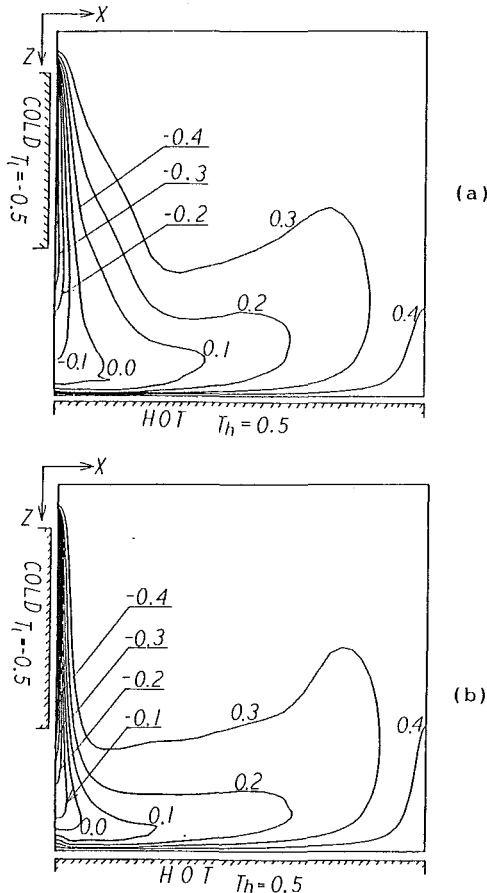

(a)

(b)

Fig. 3 Computed isothermal lines in vertical planes normal to the heated and cooled walls at Ra = 10^7 and Pr = 0.7: (a) Y = 0.05$\bar{H}$; (b) Y = 0.5$\bar{H}$

(a)

(b)

Fig. 4 Computed isothermal lines in vertical planes parallel to the cooled wall at Ra = 10^7 and Pr = 0.7: (a) X = 0.041$\bar{H}$; (b) X = 0.904$\bar{H}$

number and a strange mode of flow for two-dimensional turbulent natural convection. They therefore adopted a hybrid scheme suggested by Patankar [12] in which the upwind scheme was employed only when the matrix coefficient became negative. This scheme yielded the stable, experimentally observed mode of flow. A similar scheme was employed in this work. The numerical scheme of integration, which utilized the A.D.I. method, is the same as that of [7].

3 Computed Results

The turbulent regime begins at Gr = 10^9 for convection along a heated vertical wall in an unconfined fluid and at Ra = 2×10^4 for convection in an enclosure heated from below and cooled from above. The boundary conditions of this investigation encompass these two limiting cases. Hence the primary calculations were carried out for Ra = 10^6 and 10^7 and Pr = 0.7. The number of divisions are 20 by 10 by 10 for
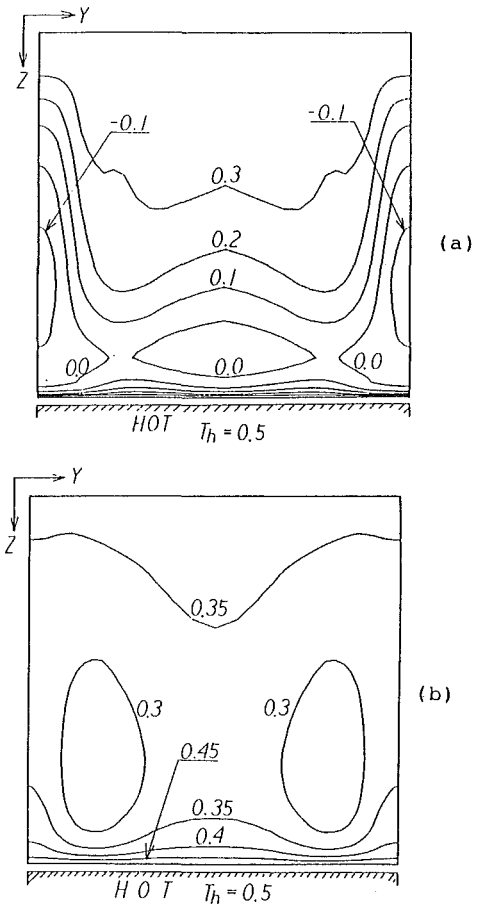
Ra = 10^6 and 24 by 10 by 14 for Ra = 10^7 in the X, Y, and Z directions, respectively. Closer spacings were employed near the surfaces except for the one in the Y direction at Ra = 10^6. The grid sizes were determined on a trial basis. At least two grid points were taken beteween the surface and the point of local peak velocity for the boundary-layer-type flow over the vertical cooled wall and over the hot horizontal floor. This scheme was based on the experience obtained from the computations for the two-dimensional turbulent natural convection by Ozoe et al. [7].

The overall Nusselt number on the heated floor and the Y component of the vector potential at the center of the region were used as a measure of convergence. The criterion of convergence was a relative change of the average Nusselt number on the heated floor of less than 10^{-4}. The Y component of the vector potential was also used as an indication of the trend of convergence. The number of iterations required for Ra = 10^6 was 1600 and for Ra = 10^7 was 1400. The initial condition for Ra = 10^6 was the numerical solution for the laminar model.

The converged overall Nusselt number on the heated floor was 6.04 at Ra = 10^6 and 13.27 at Ra = 10^7. The ratio of these two Nusselt numbers is 2.2, suggesting the proportionality of the overall Nusselt number to the 1/3 power of the Rayleigh number, as is known to hold for the turbulent regime.

Representative results, mostly for Ra = 10^7 and Pr = 0.7, are shown in graphic form as follows. The computed velocity vectors at a steady state of Ra = 10^7 and Pr = 0.7 are described in Fig. 2 for two vertical planes of constant Y. The length of the arrow represents the magnitude of the velocity projected on the indicated vertical X-Z plane. The velocity vectors at $Y = 0.21\bar{H}$ (not shown) and 0.5 $\bar{H}$ are similar to each other but that at $Y = 0.05 \bar{H}$ differs greatly due to the
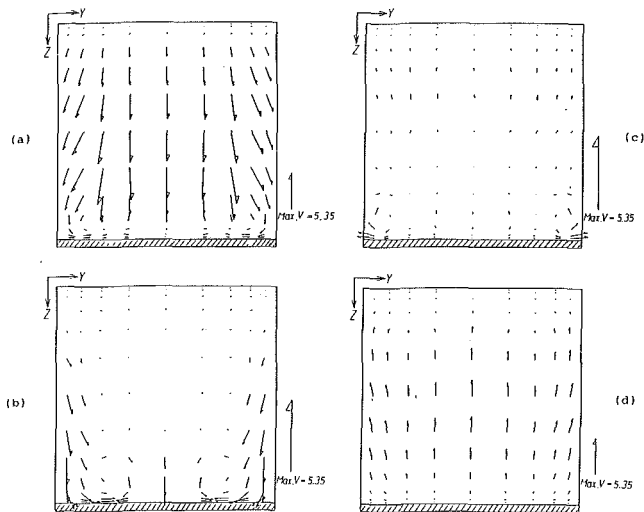
Fig. 5 Computed velocity vectors in vertical planes parallel to the cooled wall at Ra = 10^7 and Pr = 0.7: (a) X = 0.016$\bar{H}$; (b) X = 0.14$\bar{H}$; (c) X = 0.5$\bar{H}$; (d) X = 0.935 $\bar{H}$

Fig. 6 Computed velocity vectors in horizontal planes at Ra = 10^7 and Pr = 0.7: (a) Z = 0.05$\bar{H}$; (b) Z = 0.5$\bar{H}$; (c) Z = 0.79$\bar{H}$; (d) Z = 0.98$\bar{H}$

presence of the wall and the resulting three-dimensional effect. Boundary-layer-type flow can be seen along the vertical cold window and the heated floor in Fig. 2(b).

The computed isothermal lines at Ra = 10^7 and Pr = 0.7 are shown in Fig. 3 for two vertical planes of constant Y and in Fig. 4 for two vertical planes of constant X. The isothermal lines are dense over the left window due to the cooling and also over the heated floor, especially under the window. The isothermal lines at Y = 0.05$\bar{H}$ differ from those at Y = 0.5$\bar{H}$ due to the presence of the side wall. The computed isothermal lines for two vertical planes of constant X can be seen in Fig. 4. The isothermal lines are symmetric with respect to Y = 0.5$\bar{H}$ due to the symmetric boundary condition. The symmetry of the computed values about Y = 0.5$\bar{H}$ assures to some extent the reliability of the computations. A cold area prevails along the side walls at Y = 0 and $\bar{H}$ as seen in Fig. 4(a) at X = 0.041$\bar{H}$, but in Fig. 4(b) at X = 0.904$\bar{H}$ two cold areas like cat eyes appear near the rear wall. These characteristics are apparently due to the three-dimensional effects.

The three dimensionality of the flow can also be seen in the vertical view of the velocity vectors as shown in Fig. 5 for various planes of X. These vectors are those seen from the window side. The symmetry with respect to Y = 0.5$\bar{H}$ is clear. The downward velocity near the X = 0 plane is described for X = 0.016$\bar{H}$ in Fig. 5(a). Near the rear wall at X = 0.935$\bar{H}$, the flow is upward as seen in Fig. 5(d). An interesting but weak pattern of flow can be seen at X = 0.14$\bar{H}$ and 0.5$\bar{H}$ in Fig. 5(b) and Fig. 5(c), respectively. Near the side walls at Y = 0 and $\bar{H}$ in Fig. 5(c), a weak spiral motion appears to exist with its axis in the direction of the main flow.

The three dimensionality of the flow is best indicated by velocity vectors in the horizontal plane, as shown in Fig. 6 for various heights at Ra = 10^7. On the right-hand side of each graph, the arrow of the maximum velocity is drawn to indicate the relative magnitude of the velocity components. The flow pattern is symmetric with respect to the Y = 0.5$\bar{H}$ plane. The main flow near the top plane is toward the cooled window at X = 0, as seen in Fig. 6(a). Figure 6(d) shows flow in the reverse direction just above the floor, as expected from Fig. 2. However, as seen in Figs. 6(b) and 6(c) a secondary flow in the form of a spiral apparently occurs along the vertical corner over the cooled window adjacent to the two side walls. The velocity component in the Y direction is one order less than that in the X direction, and these spiral velocity components may not be strong enough to make a complete spiral at the indicated locations, even though they reveal some deflection from the main circulating flow.
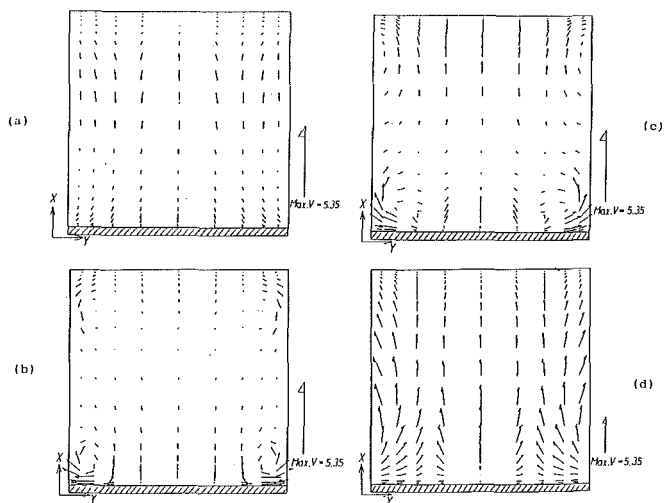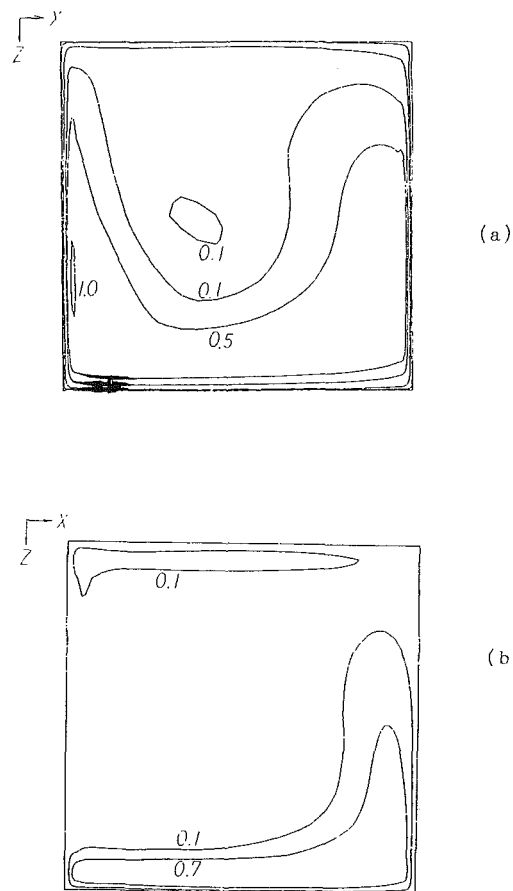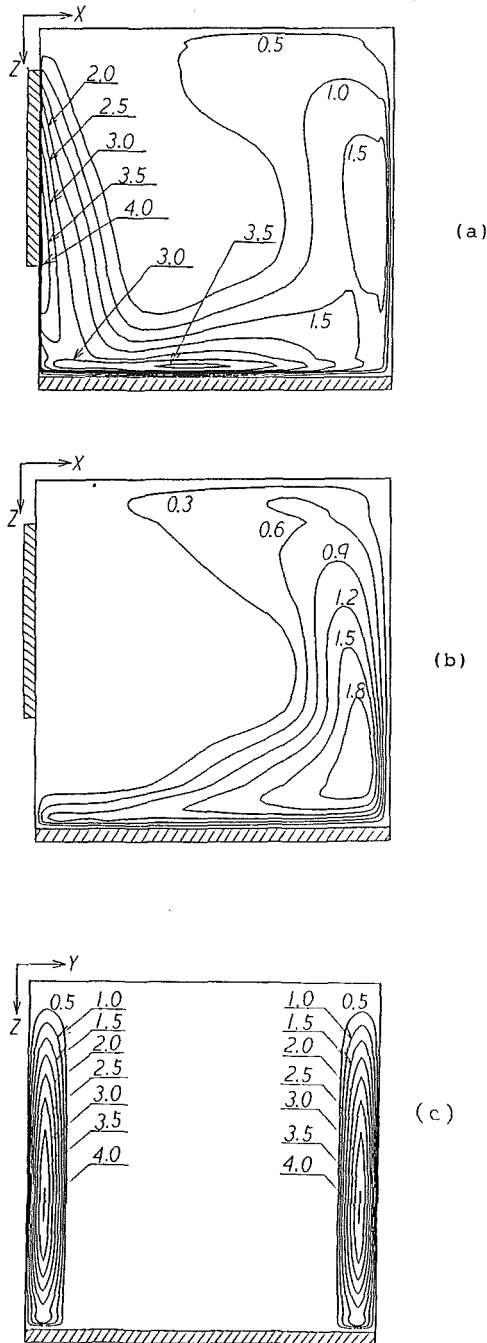

Fig. 7 Computed contours of the dimensionless eddy diffusivity in vertical planes perpendicular to the heated and cooled walls at Ra = 10^6 and Pr = 0.7: (a) Y = 0.1$\bar{H}$; (b) Y = 0.5$\bar{H}$

The turbulent intensity is not strong, and the maximum values of the dimensionless eddy diffusivity are 1.84 and 4.03 for Ra = 10^6 and 10^7, respectively. As shown in Table 1, these are 2.6 and 5.8 times the molecular kinematic viscosity. Contour maps of the eddy diffusivity at Ra = 10^6 are shown in Fig. 7, and those at Ra = 10^7 in Fig. 8. The peak value of ν_t^* occurs in the vertical plane Y = 0.1$\bar{H}$ at Ra = 10^6, and in the plane Y = 0.05$\bar{H}$ at Ra = 10^7 as shown in Figs. 7(a) and 8(a). The eddy diffusivity is also relatively large along the heated floor. Contour maps for a symmetric plane are shown in Figs. 7(b) and 8(b) for Ra = 10^6 and 10^7, respectively. The maximum eddy diffusivity probably occurs near the side
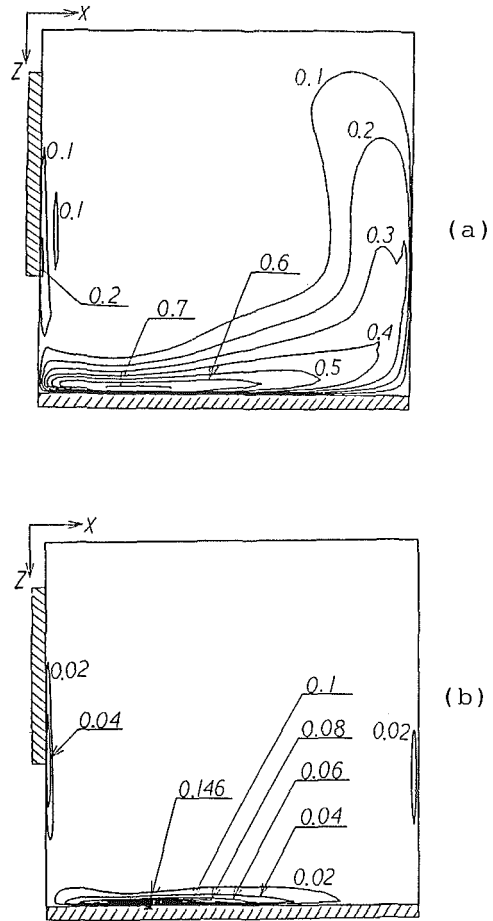
Table 1 Summary of the computed results

|	Ra = 10^6	10^7
Nu on the floor	6.04	13.27
Dimensionless maximum velocity, W	3.025	5.350
Maximum of ν_t^*	1.84	4.03
Maximum of ν_t^*/ν	2.6	5.8

(a)

(b)

(c)

Fig. 8 Computed contours of the dimensionless eddy diffusivity in vertical planes at Ra = 10^7 and Pr = 0.7: (a) Y = 0.05$\overline{H}$; (b) Y = 0.5$\overline{H}$; (c) X = 0.0046$\overline{H}$

(a)

(b)

Fig. 9 Computed contours in a vertical plane at Y = 0.5$\overline{H}$ perpendicular to the heated and cooled walls at Ra = 10^7 and Pr = 0.7: (a) dimensionless time-averaged turbulent kinetic energy; (b) dimensionless time-averaged rate of dissipation of turbulent kinetic energy
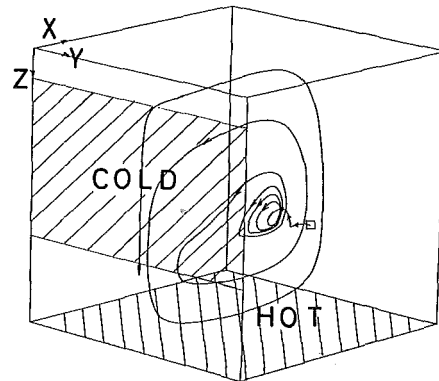
Fig. 10 Perspective view of a computed streakline for the time-averaged velocity: Ra = 10^6, Pr = 0.7; starting point (X_0, Y_0, Z_0) = (0.66$\overline{H}$, 0.7$\overline{H}$, 0.63$\overline{H}$); duration τ = 1500; eye point (X, Y, Z) = (−12$\overline{H}$, 12$\overline{H}$, −5$\overline{H}$)

wall because of the downward spiral movement seen in Figs. 6(b) and 6(c). This is more evident in the contour maps of the eddy diffusivity in a vertical plane $X = 0.0046\overline{H}$ as seen from the cold window per Fig. 8(c). The eddy diffusivity has a peak value near the side walls adjacent to the corner over the vertical cooled window. These characteristics, which were observed for both Ra = 10^6 and 10^7, confirm the importance

of three-dimensional computations for the turbulent convection.

The contour maps of the turbulent kinetic energy and the rate of dissipation of turbulent kinetic energy are shown in Fig. 9 at Ra = 10^7 and Pr = 0.7, both in the vertical plane of symmetry at $Y = 0.5\overline{H}$. The peak values of these turbulent properties occur both along the cold window and over the heated floor due to the strong shear in a fluid stream between a rigid wall and a stagnant core.

The flow characteristics can be identified more clearly from plots of streaklines than from the velocity vectors. Figure 10 is

a perspective view for Ra = 10^6 and Pr = 0.7 of the streakline for the time-averaged velocity of a particle starting from $(X_0, Y_0, Z_0) = (0.66\overline{H}, 0.7\overline{H}, 0.63\overline{H})$ as shown by the rectangular symbol. This streakline reveals the characteristic coaxial double spiral movement computed and observed experimentally by Ozoe et al. [13] for laminar natural convection in various enclosures. The particle should return to the starting point following a reduction in its radius of circulation near $Y = \overline{H}$. The axis of the strong circulating flow is not at the center of the X–Z cross section but lower and away from the cooled area due to the nonsymmetric thermal boundary conditions. The velocity is very slow at the initial, small radius of circulation due to the rather stagnant core. However, once the particle joins the main flow along the walls, its circulating velocity increases greatly. In this example, 80 percent of the time of the particle generating this streakline was spent in the central spiral of small radius. This result suggests that such a spiral movement exists for the time-averaged velocity field even in the turbulent regime in spite of significant differences in the geometric and thermal boundary conditions, and also that this spiral movement is a general characteristic of natural convection in a confined regime.

Although the computation was limited up to Ra = 10^7 due to the computational time of more than an hour, the scheme itself would be expected to be applicable at least up to Ra = 10^{11}, if a finer grid size were used, based on our experience with two-dimensional natural convection in [7].

Summary

A three-dimensional k–ϵ model for turbulent natural convection in a cubical room heated on the floor and cooled on a part of one of the vertical walls was solved numerically for Ra = 10^6 and 10^7 and Pr = 0.7. The maximum eddy diffusivity was 2.6 and 5.8 times the molecular kinematic viscosity at Ra = 10^6 and 10^7, respectively. The overall Nusselt numbers on the heated floor were 6.04 and 13.27 for Ra = 10^6 and 10^7, respectively, suggesting proportionality of the Nusselt number to the 1/3 power of the Rayleigh number.

Complicated spiral vectors were found to exist in the downward and horizontal time-averaged flows both for Ra = 10^6 and 10^7.

The computed values of all variables were found to be symmetric in terms of the central vertical plane normal to the cooled area, thus confirming to some extent the reliability of the computations. A coaxial double spiral movement, similar to that previously reported for laminar natural convection, was found for the time-averaged flow field.

The computational scheme developed herein is expected to be applicable for other thermal boundary conditions which generate turbulent three-dimensional natural convection in a confined regime.

Although the computed results in this paper are for a cubical enclosure oriented horizontally, and for a particular

set of boundary conditions, the finite-difference model is applicable for other aspect ratios, arbitrary boundary conditions, and arbitrary inclinations.

Experimental measurements apparently do not exist to test these particular computations critically. However, the model itself has been tested and found to be reliable for closely related two-dimensional convection [7].

The computations were necessarily limited by computer demands to 24 grids or fewer in each direction. However, based on tests of similar two-dimensional calculations, this grid is presumed to be sufficient to reveal the correct pattern of flow.

Acknowledgments

References

1 Plumb, O. A., and Kennedy, L. A., "Application of a k–ϵ Turbulence Model to Natural Convection From a Vertical Isothermal Surface," ASME JOURNAL OF HEAT TRANSFER, Vol. 99C, 1977, pp. 79–85.

2 Lin, S. J., and Churchill, S. W., "Turbulent Free Convection From a Vertical Isothermal Plate," *Num. Heat Transfer*, Vol. 1, 1978, pp. 129–145.

3 Fujii, M., and Fujii, T., "Numerical Calculation of Turbulent Free Convection Along a Vertical Plate," *Trans. JSME*, Vol. 43, No. 374, 1977, pp. 3825–3834; Vol. 44, No. 384, 1978, pp. 2797–2807.

4 Farouk, B., and Güceri, S. I., "Natural Convection From a Horizontal Cylinder—Turbulent Regime," ASME JOURNAL OF HEAT TRANSFER, Vol. 104C, 1982, pp. 228–235.

5 Fraikin, M. P., Portier, J. J., and Fraikin, C. J., "Application of a k–ϵ Turbulence Model to an Enclosed Buoyancy-Driven Recirculating Flow," *19th ASME-AIChE Nat. Heat Transfer Conf.*, Orlando, Florida, 1980, Paper No. 80-HT-68.

6 Farouk, B., and Güceri, S. I., "Laminar and Turbulent Natural Convection in the Annulus Between Horizontal Concentric Cylinders," ASME JOURNAL OF HEAT TRANSFER, Vol. 104, 1982, pp. 631–636.

7 Ozoe, H., Mouri, A., Ohmuro, M., Churchill, S. W., and Lior, N., "Numerical Calculations of Laminar and Turbulent Natural Convection in Water in Rectangular Channels Heated and Cooled Isothermally on the Opposing Vertical Walls," *Int. J. Heat Mass Transfer*, Vol. 28, No. 1, 1985, pp. 125–138.

8 Jones, W. P., and Launder, B. E., "The Prediction of Laminarization With a Two-Equation Model of Turbulence," *Int. J. Heat Mass Transfer*, Vol. 15, 1972, pp. 301–314.

9 Launder, B. E., and Spalding, D. B., "The Numerical Computation of Turbulent Flows," *Comp. Meth. Appl. Mech. and Eng.*, Vol. 3, 1974, pp. 269–289.

10 Hirasaki, G. J., and Hellums, J. D., "A General Formulation of the Boundary Conditions on the Vector Potential in Three-Dimensional Hydrodynamics," *Quart. Appl. Math.*, Vol. 26, 1968, pp. 331–342.

11 Kawamura, H., private communication.

12 Patankar, S. V., *Studies in Convection*, Vol. 1, B. E. Launder, ed., Academic Press, New York, 1975.

13 Ozoe, H., Sato, N., and Churchill, S. W., "Experimental Confirmation of the Three-Dimensional Helical Streaklines Previously Computed for Natural Convection in Inclined Rectangular Enclosures," *Kagaku Kogaku Ronbunshu*, Vol. 5, 1979, pp. 19–25 (in Japanese); English translation, *International Chem. Eng.*, Vol. 19, 1979, pp. 454–462.